PERGAMON

International Journal of Solids and Structures 39 (2002) 3971–3996

INTERNATIONAL JOURNAL OF SOLIDS and STRUCTURES

www.elsevier.com/locate/ijsolstr

Effects of pre-stress on crack-tip fields in elastic, incompressible solids

Enrico Radi [a,*], Davide Bigoni [b], Domenico Capuani [c]

[a] *Dipartimento di Scienze e Metodi dell'Ingegneria, Università di Modena e Reggio Emilia, Viale Allegri 13, 42100 Reggio Emilia, Italy*

[b] *Dipartimento di Ingegneria Meccanica e Strutturale, Università di Trento, Via Mesiano 77, 38050 Povo, Trento, Italy*

[c] *Dipartimento di Ingegneria, Università di Ferrara, Via Saragat 1, 44100 Ferrara, Italy*

Received 12 November 2001; received in revised form 7 March 2002

Abstract

A closed-form asymptotic solution is provided for velocity fields and the nominal stress rates near the tip of a stationary crack in a homogeneously pre-stressed configuration of a nonlinear elastic, incompressible material. In particular, a biaxial pre-stress is assumed with stress axes parallel and orthogonal to the crack faces. Two boundary conditions are considered on the crack faces, namely a constant pressure or a constant dead loading, both preserving an homogeneous ground state. Starting from this configuration, small superimposed Mode I or Mode II deformations are solved, in the framework of Biot's incremental theory of elasticity. In this way a definition of an incremental stress intensity factor is introduced, slightly different for pressure or dead loading conditions on crack faces. Specific examples are finally developed for various hyperelastic materials, including the J_2-deformation theory of plasticity. The presence of pre-stress is shown to strongly influence the angular variation of the asymptotic crack-tip fields, even if the nominal stress rate displays a square root singularity as in the infinitesimal theory. Relationships between the solution with shear band formation at the crack tip and instability of the crack surfaces are given in evidence.

Keywords: Fracture; Shear bands; Elastic material; Residual stress; Asymptotic analysis

1. Introduction

Structures made of natural and artificial materials and ranging widely in size—such as geological formations or microstructures employed in electronics—are often anisotropic and subject to severe residual stress fields (or pre-stresses). Both effects strongly influence mechanical behaviour. For instance, as connected to the possible appearance of buckled configurations, the pre-stress plays often a key role in the design of microelectromechanical systems. In this context, solutions to crack problems become particularly important. These are available under small strain hypothesis (Eshelby et al., 1953; Sih et al., 1965; Willis,

* Corresponding author. Tel.: +39-522-406356; fax: +39-522-496466.
E-mail addresses: eradi@unimo.it (E. Radi), bigoni@ing.unitn.it (D. Bigoni), cpd@dns.unife.it (D. Capuani).

PII: S0020-7683(02)00252-4

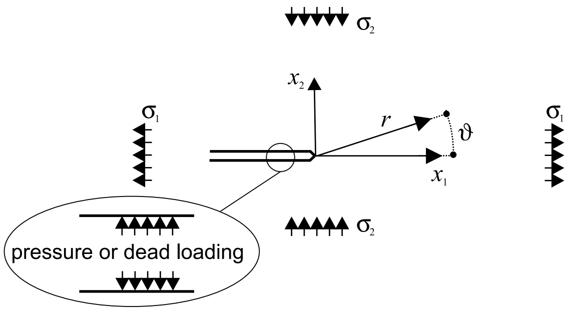

Fig. 1. Crack geometry and reference systems.

1966; Barnett and Asaro, 1972; Obata et al., 1989; Antipov et al., 2000; Azhdari et al., 2000), however the influence of pre-stress still remains almost unexplored. [1] In particular, at least to the author's knowledge, only the contributions by Soós (1996a,b) and Crăciun and Soós (1998) are available. [2] These works deserve a special mention, since many of results obtained there are confirmed in the present paper, though for a different constitutive setting and boundary conditions on crack faces.

The problem of a plane crack in a pre-stressed infinite elastic medium, undergoing arbitrary large but homogeneous and plane strain deformations, is considered in this work. A Lagrangian formulation is adopted by taking the current state as the reference configuration which is assumed in a homogeneous state defined by two stress components, one collinear with and the other orthogonal to the crack. The stress component orthogonal to the crack line is assumed to be produced by two different conditions on the crack faces, namely, assigned constant *pressure* or *dead loading* (Fig. 1). The former condition is more physically sound, but the latter is included for comparison. Starting from this plane strain configuration, where all fields are homogeneous, the effects of small superimposed Mode I and Mode II deformations are investigated. Similar to infinitesimal theory, the incremental [3] fields are governed by a single parameter—the stress intensity factor rate—and the stronger singularity (corresponding to an integrable second-order energy) has a square root dependence on crack-tip distance, as first shown in a similar context by Soós (1996a). However, while the presence of a collinear stress influences only the higher-order terms for linear elastic fracture mechanics (Rice, 1974), we show that in the context of incremental elastic deformations, the leading-order terms result to be strongly influenced by the pre-stress. In addition, we will show that the two different boundary conditions on crack faces lead to the introduction of two different incremental stress intensity factors and related incremental versions of the conserved integrals. It is also shown that the asymptotic crack-tip rate fields become unbounded, when the pre-stress in the current configuration approaches the critical value of surface instability. This usually occurs within the elliptic regime and terminates the homogeneous response of the body. When the threshold for surface instability is close enough to the elliptic boundary, we show that the asymptotic fields tend to self-organize along localized patterns of deformation, a fact fully consistent with findings by Bigoni and Capuani (2002).

It is worth mentioning that, starting from Wong and Shield (1969) and Knowles and Sternberg (1973, 1974), a number of analyses were performed in the framework of nonlinear elasticity, in which a crack is

[1] With "pre-stress in elasticity" we mean that small deformations are superimposed upon a state of initial stress, in the context of a fully nonlinear theory of elasticity (Ogden, 1984). Therefore, the approach followed here turns out to be substantially different from a mere superposition of elastic fields, which may retain validity when the initial stress is small compared with, say, the elastic shear modulus (see, e.g. Lawn and Marshall, 1977; Green and Maloney, 1986).

[2] Soós also mentions books (in Russian) by A.N. Guz, not available to us.

[3] All results that will be presented hold true for an incremental theory or for a rate theory. Therefore, the words "rates" and "increments" will be used as synonyms.

considered loaded from a *stress-free state* (Stephenson, 1982; Le and Stumpf, 1993; Geubelle and Knauss, 1994; Geubelle, 1995). An important difference with the present work lies in that assumption that is removed here, though with reference to the incremental problem only. It may be important also to mention that Geubelle (1995) shows that the singularities of the Cauchy and nominal stresses are different for a neo-Hookean material, so that the near-tip stress fields behave as $r^{-1/2}$ and r^{-1} respectively, and the displacement field as $r^{1/2}$ (where r is the distance from the crack tip).

The present article is organized as follows. The field and constitutive equations are recalled in Section 2, adopting the Hill and Hutchinson (1975) and Young (1976) formalism to describe the Biot (1965) model for incompressible and orthotropic incremental elasticity. In Section 3, following the approach employed by Piva and Radi (1991) and Loret and Radi (2001) for the analysis of crack propagation in linear elastic and poroelastic materials, a complex variable formulation is adopted to solve the field equations expressed in terms of a stream function. An asymptotic analysis is performed—restricted to the elliptic regime—to describe the leading-order term of the stream function close to the crack tip. In Section 4, the leading-order terms of the various fields are obtained in a closed form for the case of elliptic imaginary and elliptic complex regimes, both for Mode I and Mode II loading conditions. Conserved integrals for incremental quantities are introduced in Section 5, where it is shown that a formulation is needed in terms of a particular, say, "fictitious" stress rate, when pressure loading boundary conditions on crack faces are considered. Finally, examples are given in Section 6. In particular, a tensile or compressive pre-stress collinear with the crack is considered (i.e. the crack faces are traction free). The strong quantitative and qualitative effect of pre-stress on near tip fields is demonstrated.

2. Governing equations

Plane strain incremental displacements v_i, satisfying the incompressibility constraint

$$v_{1,1} + v_{2,2} = 0, \tag{2.1}$$

are superimposed upon a given homogeneous, finitely deformed nonlinear elastic body. In a Lagrangian formulation with the current state taken as reference, the incremental stress response in terms of nominal stress tensor t_{ij} can be written in the form (Biot, 1965; Hill and Hutchinson, 1975):

$$\begin{aligned} \dot{t}_{11} &= \mu(2\xi - k - \eta)v_{1,1} + \dot{p}, \\ \dot{t}_{22} &= \mu(2\xi + k - \eta)v_{2,2} + \dot{p}, \\ \dot{t}_{12} &= \mu[(1+k)v_{2,1} + (1-\eta)v_{1,2}], \\ \dot{t}_{21} &= \mu[(1-\eta)v_{2,1} + (1-k)v_{1,2}], \end{aligned} \tag{2.2}$$

where μ is the incremental modulus corresponding to shearing parallel to the principal stress axes and

$$\xi = \frac{\mu_*}{\mu}, \quad \eta = \frac{p}{\mu} = \frac{\sigma_1 + \sigma_2}{2\mu}, \quad k = \frac{\sigma_1 - \sigma_2}{2\mu}, \tag{2.3}$$

in which μ_* is the incremental modulus corresponding to shearing inclined at 45° to the principal stress axes, p is the in-plane hydrostatic stress and σ_1 and σ_2 are the principal values of the Cauchy stress tensor. This is related to the nominal stress through $\sigma_{ij} = J^{-1}F_{ik}t_{kj}$, with F_{ik} being the deformation gradient and J its determinant, equal to unit here as a consequence of incompressibility.

When a homogeneous current state is considered, it may be shown that the rate field equations deriving from equilibrium, namely $\dot{t}_{ij,i} = 0$, imply:

$$\begin{aligned}\dot{p}_{,1} &= \mu[(1+k-2\xi)v_{1,11}-(1-k)v_{1,22}],\\ \dot{p}_{,2} &= \mu[(1-k-2\xi)v_{2,22}-(1+k)v_{2,11}].\end{aligned} \tag{2.4}$$

The above formulation describes a broad class of constitutive relations, including the relevant cases of Mooney-Rivlin, Ogden and J_2–deformation materials (Ogden, 1984; Hutchinson and Neale, 1978).

By introducing a stream function $\psi(x_1, x_2)$ such that the incompressibility condition (2.1) is automatically satisfied:

$$v_1 = \psi_{,2}, \quad v_2 = -\psi_{,1}, \tag{2.5}$$

the conditions (2.4) yield (Hill and Hutchinson, 1975):

$$(1+k)\psi_{,1111} + 2(2\xi-1)\psi_{,1122} + (1-k)\psi_{,2222} = 0. \tag{2.6}$$

Similar to small strain anisotropic elasticity (Lekhnitskii, 1981), it is instrumental to assume the stream function in the form:

$$\psi(x_1, x_2) = AF(x_1 + \Omega x_2), \tag{2.7}$$

where A and Ω are complex constants and F is an analytic function of its complex argument. The constant Ω will be shown to be real or complex, depending on the parameters ξ and k. In fact, a substitution of (2.7) into (2.6) yields the following biquadratic equation for Ω:

$$(1-k)\Omega^4 + 2(2\xi-1)\Omega^2 + 1 + k = 0. \tag{2.8}$$

The roots Ω_j $(j = 1, 2, 3, 4)$ of Eq. (2.8) verify:

$$\Omega_j^2 = \frac{1 - 2\xi + (-1)^j\sqrt{4\xi^2 - 4\xi + k^2}}{1-k}, \tag{2.9}$$

and turns out to be real or complex depending on the values of ξ and k. We will restrict the analysis to the case $\xi > 0$ and $k^2 < 1$, so that three possibilities arise, which can be classified as follows.

2.1. Elliptic imaginary regime (EI):

If $2\xi > 1 + (1-k^2)^{1/2}$, Eq. (2.8) admits four purely imaginary roots, namely

$$\Omega_1 = \mathrm{i}\beta_1, \quad \Omega_2 = \mathrm{i}\beta_2, \quad \Omega_3 = \overline{\Omega}_1, \quad \Omega_4 = \overline{\Omega}_2, \tag{2.10}$$

being $\mathrm{i} = \sqrt{-1}$ and:

$$\left.\begin{matrix}\beta_1\\ \beta_2\end{matrix}\right\} = \sqrt{\frac{2\xi - 1 \pm \sqrt{4\xi^2 - 4\xi + k^2}}{1-k}}. \tag{2.11}$$

2.2. Elliptic complex regime (EC):

If $1 - (1-k^2)^{1/2} < 2\xi < 1 + (1-k^2)^{1/2}$, Eq. (2.8) admits four complex conjugate roots, namely:

$$\Omega_1 = -\alpha + \mathrm{i}\beta, \quad \Omega_2 = \alpha + \mathrm{i}\beta, \quad \Omega_3 = \overline{\Omega}_1, \quad \Omega_4 = \overline{\Omega}_2, \tag{2.12}$$

where

$$\left.\begin{matrix}\beta\\ \alpha\end{matrix}\right\} = \sqrt{\frac{\sqrt{1-k^2} \pm (2\xi - 1)}{2(1-k)}}. \tag{2.13}$$

2.3. Hyperbolic regime (H)

If $2\xi < 1 - (1-k^2)^{1/2}$, Eq. (2.8) admits four real roots, namely

$$\Omega_1 = \alpha_1, \quad \Omega_2 = \alpha_2, \quad \Omega_3 = -\Omega_1, \quad \Omega_4 = -\Omega_2, \tag{2.14}$$

being

$$\left.\begin{matrix}\alpha_1 \\ \alpha_2\end{matrix}\right\} = \sqrt{\frac{1 - 2\xi \pm \sqrt{4\xi^2 - 4\xi + k^2}}{1-k}}. \tag{2.15}$$

The condition $k^2 > 1$, not considered here, defines the parabolic regime, where Eq. (2.8) admits two real roots only. The regimes are labeled in Fig. 2, in the plane $k - \xi$.

For each of the above cases, reference is made to the four complex variables:

$$z_j = x_1 + \Omega_j x_2 = x_1 + \alpha_j x_2 + \mathrm{i}\beta_j x_2 \quad (j = 1, 2, 3, 4), \tag{2.16}$$

where $\alpha_j = \mathrm{Re}[\Omega_j]$ and $\beta_j = \mathrm{Im}[\Omega_j]$ and Re and Im denote the real and imaginary parts of a complex number, respectively. The complex variable z_j defined in (2.16) also admits the polar representation:

$$z_j = r_j \exp(\mathrm{i}\vartheta_j), \tag{2.17}$$

where

$$\begin{aligned} r_j &= \sqrt{(x_1 + \alpha_j x_2)^2 + \beta_j^2 x_2^2} = r\sqrt{(\cos\vartheta + \alpha_j \sin\vartheta)^2 + \beta_j^2 \sin^2\vartheta}, \\ \tan\vartheta_j &= \frac{\beta_j x_2}{x_1 + \alpha_j x_2} = \frac{\beta_j \sin\vartheta}{\cos\vartheta + \alpha_j \sin\vartheta}, \end{aligned} \tag{2.18}$$

in which r and ϑ are the polar coordinates of a generic point (Fig. 1). It will be useful later to refer to the following formulas for a generic power s of the variable z_j:

$$\mathrm{Re}[z_j^s] = r_j^s \cos s\vartheta_j, \quad \mathrm{Im}[z_j^s] = r_j^s \sin s\vartheta_j. \tag{2.19}$$

Owing to representation (2.7), the general solution of Eq. (2.6) may be written in the following form:

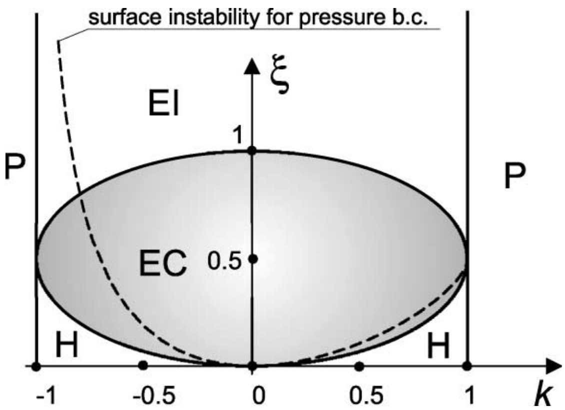

Fig. 2. Regime classification (elliptic imaginary and complex, hyperbolic and parabolic) in the k–ξ plane. Surface instability, Eq. (3.16), is shown broken.

$$\psi(x_1,x_2) = \frac{2\dot{K}}{3\mu\sqrt{\pi}}\sum_{j=1}^{4} A_jF_j(z_j), \tag{2.20}$$

where $\dot{K}$ is an amplitude factor.

Let us introduce now the problem of a semi-infinite plane crack in an infinite elastic medium (Fig. 1). A Cartesian coordinate system (x_1, x_2, x_3) and a cylindrical co-ordinate system (r, ϑ, x_3) both centered at the crack tip are considered, with the out-of-plane x_3-axis lying along the straight crack front. The current configuration is assumed to be a homogeneous state defined by a stress component σ_1 collinear with the crack and an orthogonal stress component σ_2. Two different boundary conditions are considered on the crack faces $(x_1 < 0, x_2 = 0)$:

(fixed) pressure loading:

$$\dot{t}_{22}(x_1,0) = -\sigma_2 v_{2,2}, \quad \dot{t}_{21}(x_1,0) = -\sigma_2 v_{2,1}, \tag{2.21}$$

dead loading:

$$\dot{t}_{22}(x_1,0) = 0, \quad \dot{t}_{21}(x_1,0) = 0. \tag{2.22}$$

The conditions (2.21) can be found for instance in Ogden (1984) and become *homogeneous conditions* in the variable

$$\tilde{t}_{ij} = \dot{t}_{ij} + \sigma_2 v_{i,j}, \tag{2.23}$$

representing a "fictitious stress rate", which, interestingly, satisfies the condition $\tilde{t}_{ij,i} = 0$ (due to incompressibility and homogeneity of σ_2). As will clearly appear later, the homogeneity of boundary conditions is essential in the definition of $\dot{K}$ and in the related conserved integrals. Consequently, we define the stress-intensity factor increment, namely, $\dot{K} = \dot{K}_{\mathrm{I}}$ for Mode I and $\dot{K} = \dot{K}_{\mathrm{II}}$ for Mode II as follows:

$$\dot{K}_{\mathrm{I}} = \lim_{r\to 0}\sqrt{2\pi r}\,\tilde{t}_{22}(r,\vartheta=0), \quad \dot{K}_{\mathrm{II}} = \lim_{r\to 0}\sqrt{2\pi r}\,\tilde{t}_{21}(r,\vartheta=0), \tag{2.24}$$

in which $\tilde{t}_{ij} = \dot{t}_{ij} + \sigma_2 v_{i,j}$ if the pressure loading condition (2.21) is imposed on the crack faces or $\tilde{t}_{ij} = \dot{t}_{ij}$ if the dead loading condition is prescribed.

In a neighborhood of the crack tip, the leading-order terms dominate the asymptotic expansion of the stress rate and velocity fields. Hence, within this region, the function F_j may be sought in a power form

$$F_j(z_j) = z_j^{\gamma} \quad \Rightarrow \quad \psi(x_1,x_2) = \frac{2\dot{K}}{3\mu\sqrt{\pi}}\sum_{j=1}^{4} A_j z_j^{\gamma}, \tag{2.25}$$

where γ is a real number to be obtained, together with the constants A_j, by imposing the following conditions:

(i) the stream function must be real valued;
(ii) the "fictitious" (2.21) or nominal traction (2.22) increments must vanish on the crack surface at $x_2 = 0$ and $x_1 < 0$:

$$\tilde{t}_{22}(x_1,0) = 0, \quad \tilde{t}_{21}(x_1,0) = 0. \tag{2.26}$$

(iii) the velocity field must obey Mode I or Mode II symmetry conditions:

$$v_1(x_1,x_2) = v_1(x_1,-x_2), \quad v_2(x_1,x_2) = -v_2(x_1,-x_2), \tag{2.27}$$

for Mode I loading, and

$$v_1(x_1,x_2) = -v_1(x_1,-x_2), \quad v_2(x_1,x_2) = v_2(x_1,-x_2), \tag{2.28}$$

for Mode II loading.

3. Asymptotic crack-tip fields in the elliptic imaginary regime

In the elliptic imaginary regime $\alpha_j = 0$ and, thus, from (2.10) and (2.16) it follows that

$$z_n = x_1 + \mathrm{i}\beta_n x_2 \ \ (n = 1, 2), \quad z_3 = \bar{z}_1, \quad z_4 = \bar{z}_2. \tag{3.1}$$

Moreover, by using (3.1) and noting that $\bar{z}^\gamma = \overline{z^\gamma}$, the condition (i) that the stream function (2.20) must be real valued implies $A_3 = \overline{A_1}$ and $A_4 = \overline{A_2}$, so that it may be written as

$$\psi(x_1, x_2) = \frac{4\dot{K}}{3\mu\sqrt{\pi}} \sum_{n=1}^{2} \mathrm{Re}[A_n z_n^\gamma], \tag{3.2}$$

where $A_n = a_n + \mathrm{i}b_n$ $(n = 1, 2)$, being a_n and b_n real constants. It follows that the velocity components may be obtained from (2.5) as:

$$v_1 = -\frac{4\gamma\dot{K}}{3\mu\sqrt{\pi}} \sum_{n=1}^{2} \beta_n \,\mathrm{Im}[A_n z_n^{\gamma-1}], \quad v_2 = -\frac{4\gamma\dot{K}}{3\mu\sqrt{\pi}} \sum_{n=1}^{2} \mathrm{Re}[A_n z_n^{\gamma-1}]. \tag{3.3}$$

A substitution of (3.3) into the first and second terms of expressions (2.2) of the nominal stress rates yields:

$$\begin{aligned} \dot{t}_{11} &= -\frac{4\gamma\dot{K}}{3\sqrt{\pi}}(\gamma-1)(2\xi - k - \eta) \sum_{n=1}^{2} \beta_n \,\mathrm{Im}[A_n z_n^{\gamma-2}] + \dot{p}, \\ \dot{t}_{22} &= \frac{4\gamma\dot{K}}{3\sqrt{\pi}}(\gamma-1)(2\xi + k - \eta) \sum_{n=1}^{2} \beta_n \,\mathrm{Im}[A_n z_n^{\gamma-2}] + \dot{p}. \end{aligned} \tag{3.4}$$

The hydrostatic stress rate may accordingly be assumed in the form

$$\dot{p} = \frac{4\gamma\dot{K}}{3\sqrt{\pi}}(\gamma-1) \sum_{n=1}^{2} \delta_n \beta_n \,\mathrm{Im}[A_n z_n^{\gamma-2}], \tag{3.5}$$

where the coefficients δ_1 and δ_2 may be determined by fulfillment of (2.4) as:

$$\delta_n = 2\xi - 1 - k - (1-k)\beta_n^2 \quad (n = 1, 2). \tag{3.6}$$

The complete expressions for the nominal stress rates then follows from (3.4), (3.5), (3.6) and third and fourth terms of (2.2)

$$\begin{aligned} \dot{t}_{11} &= -\frac{4\gamma\dot{K}}{3\sqrt{\pi}}(\gamma-1) \sum_{n=1}^{2} \varepsilon_n \beta_n \,\mathrm{Im}[A_n z_n^{\gamma-2}], \\ \dot{t}_{22} &= \frac{4\gamma\dot{K}}{3\sqrt{\pi}}(\gamma-1) \sum_{n=1}^{2} \chi_n \beta_n \,\mathrm{Im}[A_n z_n^{\gamma-2}], \\ \dot{t}_{12} &= -\frac{4\gamma\dot{K}}{3\sqrt{\pi}}(\gamma-1) \sum_{n=1}^{2} \chi_n \beta_n^2 \,\mathrm{Re}[A_n z_n^{\gamma-2}], \\ \dot{t}_{21} &= -\frac{4\gamma\dot{K}}{3\sqrt{\pi}}(\gamma-1) \sum_{n=1}^{2} \varepsilon_n \,\mathrm{Re}[A_n z_n^{\gamma-2}], \end{aligned} \tag{3.7}$$

where

$$\varepsilon_n = 1 - \eta + (1-k)\beta_n^2, \quad \chi_n = 4\xi - 1 - \eta - (1-k)\beta_n^2. \tag{3.8}$$

Note that relations (3.8) and (2.11) imply the following conditions

$$\varepsilon_1 = \chi_2, \quad \varepsilon_2 = \chi_1, \tag{3.9}$$

which have been used in (3.7).

3.1. Mode I symmetry conditions

Under Mode I loading conditions, in view of (2.27) and (3.1), the velocity fields (3.3) must be endowed with the symmetry properties:

$$v_1(z_1, z_2) = v_1(\bar{z}_1, \bar{z}_2), \quad v_2(z_1, z_2) = -v_2(\bar{z}_1, \bar{z}_2), \tag{3.10}$$

which imply $a_1 = a_2 = 0$, so that:

$$A_n = \mathrm{i}b_n \quad (n = 1, 2). \tag{3.11}$$

When the boundary conditions (2.26) at the crack faces ($\vartheta = \pi$ or, equivalently, $\vartheta_n = \pi$) are imposed using the nominal stress rates (second and fourth terms of (3.7)) and the velocity gradient calculated from (3.3), the following homogeneous system for the real constants b_1 and b_2 may be obtained by using relations (2.19) and (3.11):

$$\left(\sum_{n=1}^{2} b_n \tilde{\chi}_n \beta_n\right) \cos(\gamma\pi) = 0, \quad \left(\sum_{n=1}^{2} b_n \tilde{\varepsilon}_n\right) \sin(\gamma\pi) = 0. \tag{3.12}$$

where $\tilde{\chi}_n = \chi_n + \sigma_{22}/\mu$ and $\tilde{\varepsilon}_n = \varepsilon_n + \sigma_{22}/\mu$ for pressure loading (2.21) or $\tilde{\chi}_n = \chi_n$ and $\tilde{\varepsilon}_n = \varepsilon_n$ for dead loading (2.22).

If the surface instability condition

$$\tilde{\varepsilon}_2^2 \beta_1 - \tilde{\varepsilon}_1^2 \beta_2 = 0, \tag{3.13}$$

is excluded, system (3.12) admits a nontrivial solution for the constants b_1 and b_2 if and only if

$$\sin(2\gamma\pi) = 0. \tag{3.14}$$

Similar to the infinitesimal theory, we assume here that the second-order strain energy $\dot{t}_{ij} v_{j,i}/2$ be integrable in a neighborhood of the crack tip, so that the set of values of γ satisfying both integrability and condition (3.14) is $\gamma = 3/2, 2, 5/2, \ldots$ The lowest admissible value $\gamma = 3/2$ leads to the square root singularity of the local crack-tip fields for the nominal and hydrostatic stress rates. This result agrees with the findings of finite elasticity investigations (Geubelle, 1995) for neo-Hookean material.

After algebraic manipulations, it can be shown that the condition (3.13) occurs for a critical value k defined by

$$k^2 = 1 - \left[\sqrt{(2\xi - \tilde{\eta})^2 + (1 - \tilde{\eta})^2} \pm (2\xi - \tilde{\eta})\right]^2, \tag{3.15}$$

where $\tilde{\eta} = k$ for pressure loading (2.21) or $\tilde{\eta} = \eta$ for dead loading (2.22). Eq. (3.15) represent the condition for surface instability and is equivalent to Eq. (48) of Needleman and Ortiz (1991) for dead loading boundary conditions. Assuming pressure loading boundary condition, $\tilde{\eta} = k$ (which holds true even in the trivial case of traction-free crack faces, $\sigma_2 = 0$), Eq. (3.15) becomes

$$\xi = \frac{k}{2}\left(1 - \sqrt{\frac{1-k}{1+k}}\right), \tag{3.16}$$

corresponding to the dashed curve in the EI regime plotted in Fig. 2. When $k = \sigma_1/(2\mu)$, Eq. (3.16) coincides with the bifurcation condition for a semi-infinite block under plane strain tension or compression test, as found by Hill and Hutchinson (1975, Eq. (6.5)) and Young (1976, Eq. (5.37)), respectively. Note that Eq. (3.16) is independent of η, a circumstance noted also by Dowaikh and Ogden (1990) and in the context of wave propagation.

Referring to pressure loading conditions, it is important to note from Fig. 2 that—*in a continuous path starting within* (E)—*the* (EI)/(P) *boundary in tension is the only portion of the* (E) *boundary attainable without encountering a surface instability*. In the problem under consideration, surface instability corresponds to instability of the crack faces, so that combinations of parameters corresponding to states beyond the surface instability threshold do not represent relevant physical situations and therefore will not be considered.

If the condition (3.13) is excluded and for $\gamma = 3/2$, the second term of the condition (3.12) on the crack faces, yields the following constraint between the constants b_1 and b_2:

$$\sum_{n=1}^{2} b_n \tilde{\varepsilon}_n = 0. \tag{3.17}$$

Therefore, the leading-order contributions of the various fields can be expressed in terms of the stress-intensity factor rate $\dot{K}_{\mathrm{I}}$ for Mode I loading conditions defined in (2.24). Correspondingly, the velocity and stress rate fields can be written in the form:

$$\boldsymbol{v}(r,\vartheta) = \frac{\dot{K}_{\mathrm{I}}}{\mu}\sqrt{\frac{r}{2\pi}}\boldsymbol{\omega}(\vartheta), \quad \dot{\boldsymbol{t}}(r,\vartheta) = \frac{\dot{K}_{\mathrm{I}}}{\sqrt{2\pi r}}\boldsymbol{\tau}(\vartheta), \quad \dot{p}(r,\vartheta) = \frac{\dot{K}_{\mathrm{I}}}{\sqrt{2\pi r}}\rho(\vartheta), \tag{3.18}$$

where the functions $\boldsymbol{\omega}(\vartheta)$, $\boldsymbol{\tau}(\vartheta)$ and $\rho(\vartheta)$ denote the variation with the angular coordinate ϑ of velocity, nominal and hydrostatic stress rates. In particular, by introducing the expression (3.11) of the constant A_n for Mode I loading conditions into the expressions (3.3), (3.5) and (3.7) of the rate fields, the angular functions defined in (3.18) assume the following analytical expressions, valid for $\vartheta \in [0, \pi]$:

$$\begin{aligned}
\omega_1(\vartheta) &= -2\sum_{n=1}^{2} b_n\beta_n\sqrt{g_n(\vartheta)+\cos\vartheta}, \\
\omega_2(\vartheta) &= 2\sum_{n=1}^{2} b_n\sqrt{g_n(\vartheta)-\cos\vartheta}, \\
\tau_{11}(\vartheta) &= -\sum_{n=1}^{2} b_n\varepsilon_n\beta_n\sqrt{g_n(\vartheta)+\cos\vartheta}/g_n(\vartheta), \\
\tau_{22}(\vartheta) &= \sum_{n=1}^{2} b_n\chi_n\beta_n\sqrt{g_n(\vartheta)+\cos\vartheta}/g_n(\vartheta), \\
\tau_{12}(\vartheta) &= -\sum_{n=1}^{2} b_n\chi_n\beta_n^2\sqrt{g_n(\vartheta)-\cos\vartheta}/g_n(\vartheta), \\
\tau_{21}(\vartheta) &= -\sum_{n=1}^{2} b_n\varepsilon_n\sqrt{g_n(\vartheta)-\cos\vartheta}/g_n(\vartheta), \\
\rho(\vartheta) &= \sum_{n=1}^{2} b_n\delta_n\beta_n\sqrt{g_n(\vartheta)+\cos\vartheta}/g_n(\vartheta),
\end{aligned} \tag{3.19}$$

being

$$g_n(\vartheta) = \sqrt{\cos^2\vartheta + \beta_n^2 \sin^2\vartheta}. \tag{3.20}$$

Moreover, the first term of definition (2.24) of $\dot{K}_{\mathrm{I}}$ implies the normalization condition:

$$\tilde{\tau}_{22}(0) = 1, \tag{3.21}$$

where

$$\tilde{\tau}_{22}(0) = \tau_{22}(0) + \frac{\sigma_2}{\mu}\omega_2'(0),$$

for pressure loading (2.21) or $\tilde{\tau}_{22}(0) = \tau_{22}(0)$ for dead loading (2.22) on the crack faces. We remark here that normalization (3.21) is less arbitrary than it may appear. In fact, condition (3.13) can be rewritten as $\tilde{\tau}_{22}(0) = 0$ so that the normalization condition cannot be imposed when condition (3.13) is verified. As a consequence, the choice (3.21) follows.

Using the fourth term of (3.19) and (3.17) and the relation

$$v_{2,2}(\vartheta) = \frac{\dot{K}_{\mathrm{I}}}{\mu\sqrt{2\pi r}} \sum_{n=1}^{2} b_n \beta_n \sqrt{g_n(\vartheta) + \cos\vartheta}/g_n(\vartheta),$$

for the pressure loading, the following expression may be obtained for the constants b_1 and b_2:

$$b_n = \frac{\tilde{\varepsilon}_m}{\sqrt{2}(\tilde{\varepsilon}_m^2\beta_n - \tilde{\varepsilon}_n^2\beta_m)} \quad (n, m = 1, 2;\ \ m \neq n), \tag{3.22}$$

which diverges as the condition (3.13) is approached.

3.2. Mode II symmetry conditions

Under mode II loading conditions, in view of (2.28) and (3.1), the velocity fields (3.3) meet the following symmetry properties:

$$v_1(z_1, z_2) = -v_1(\bar{z}_1, \bar{z}_2), \quad v_2(z_1, z_2) = v_2(\bar{z}_1, \bar{z}_2), \tag{3.23}$$

implying $b_1 = b_2 = 0$, so that:

$$A_n = a_n \quad (n = 1, 2). \tag{3.24}$$

When the second and fourth terms of expressions (3.7) are introduced into the boundary conditions (2.26) on the crack faces at $\vartheta = \pi$, namely for $\vartheta_n = \pi$, by using relations (2.19) and (3.24) the following homogeneous system for the real constants a_1 and a_2 may be obtained:

$$\left(\sum_{n=1}^{2} a_n \tilde{\chi}_n \beta_n\right) \sin(\gamma\pi) = 0, \quad \left(\sum_{n=1}^{2} a_n \tilde{\varepsilon}_n\right) \cos(\gamma\pi) = 0. \tag{3.25}$$

If the condition (3.13) is excluded, system (3.25) admits a nontrivial solution for the constants a_1 and a_2 if and only if condition (3.14) is satisfied. In this case, the lowest admissible value for γ is 3/2, which leads to the square root singularity of the local crack-tip fields for the nominal and hydrostatic stress rates. For $\gamma = 3/2$, the first term of condition (3.25) yields the following constraint between the constants a_1 and a_2:

$$\sum_{n=1}^{2} a_n \tilde{\chi}_n \beta_n = 0. \tag{3.26}$$

Similar to the approach adopted for the Mode I loading conditions, the leading-order contributions of the asymptotic fields can be expressed in terms of the stress-intensity factor rate $\dot{K}_{\mathrm{II}}$ for Mode II loading conditions defined in (2.24). Therefore, introducing the angular functions $\boldsymbol{\omega}(\vartheta)$, $\boldsymbol{\tau}(\vartheta)$ and $\rho(\vartheta)$, the velocity and stress rate fields can be written in the form

$$\boldsymbol{v}(r,\vartheta) = \frac{\dot{K}_{\mathrm{II}}}{\mu}\sqrt{\frac{r}{2\pi}}\boldsymbol{\omega}(\vartheta), \quad \dot{\boldsymbol{t}}(r,\vartheta) = \frac{\dot{K}_{\mathrm{II}}}{\sqrt{2\pi r}}\boldsymbol{\tau}(\vartheta), \quad \dot{p}(r,\vartheta) = \frac{\dot{K}_{\mathrm{II}}}{\sqrt{2\pi r}}\rho(\vartheta), \tag{3.27}$$

where

$$\begin{aligned}
\omega_1(\vartheta) &= -2\sum_{n=1}^{2} a_n\beta_n\sqrt{g_n(\vartheta)-\cos\vartheta},\\
\omega_2(\vartheta) &= -2\sum_{n=1}^{2} a_n\sqrt{g_n(\vartheta)+\cos\vartheta},\\
\tau_{11}(\vartheta) &= \sum_{n=1}^{2} a_n\varepsilon_n\beta_n\sqrt{g_n(\vartheta)-\cos\vartheta}/g_n(\vartheta),\\
\tau_{22}(\vartheta) &= -\sum_{n=1}^{2} a_n\chi_n\beta_n\sqrt{g_n(\vartheta)-\cos\vartheta}/g_n(\vartheta),\\
\tau_{12}(\vartheta) &= -\sum_{n=1}^{2} a_n\chi_n\beta_n^2\sqrt{g_n(\vartheta)+\cos\vartheta}/g_n(\vartheta),\\
\tau_{21}(\vartheta) &= -\sum_{n=1}^{2} a_n\varepsilon_n\sqrt{g_n(\vartheta)+\cos\vartheta}/g_n(\vartheta),\\
\rho(\vartheta) &= -\sum_{n=1}^{2} a_n\delta_n\beta_n\sqrt{g_n(\vartheta)-\cos\vartheta}/g_n(\vartheta),
\end{aligned} \tag{3.28}$$

being $g_n(\vartheta)$ already defined by (3.20). Moreover, the definition (2.24) of $\dot{K}_{\mathrm{II}}$ implies the normalization condition

$$\tilde{\tau}_{21}(0) = 1, \tag{3.29}$$

where

$$\tilde{\tau}_{21}(0) = \tau_{21}(0) + \frac{\sigma_2}{2\mu}\omega_2(0),$$

for pressure loading (2.21) or $\tilde{\tau}_{21}(0) = \tau_{21}(0)$ for dead loading (2.22) on the crack faces. Finally, by using the sixth term of (3.28) and (3.26),

$$v_{2,1}(\vartheta) = -\frac{\dot{K}_{\mathrm{II}}}{\mu\sqrt{2\pi r}}\sum_{n=1}^{2} a_n\sqrt{g_n(\vartheta)+\cos\vartheta}/g_n(\vartheta),$$

for pressure loading, the following expression may be obtained for the constants a_1 and a_2:

$$a_n = \frac{\tilde{\varepsilon}_n\beta_m}{\sqrt{2}(\tilde{\varepsilon}_m^2\beta_n - \tilde{\varepsilon}_n^2\beta_m)} \quad (n,m = 1,2;\ \ m \neq n), \tag{3.30}$$

diverging as the condition (3.13) is approached.

4. Asymptotic crack-tip fields in the elliptic complex regime

In the elliptic complex regime, the complex variables defined in (2.16) admit the following representation:

$$z_n = x_1 + (-1)^n \alpha x_2 + \mathrm{i}\beta x_2 \quad (n = 1, 2), \quad z_3 = \bar{z}_1, \quad z_4 = \bar{z}_2. \tag{4.1}$$

where α and β have been defined in (2.13). Moreover, the condition that the stream function (2.20) must assume real values only, by using (4.1) and noting that $\bar{z}^\gamma = \overline{z^\gamma}$, implies $A_3 = \overline{A_1}$ and $A_4 = \overline{A_2}$, so that the stream function may still be written in the form (3.2). In this case, the velocity components may be obtained from (2.5) as:

$$\begin{aligned} v_1 &= \frac{4\gamma\dot{K}}{3\mu\sqrt{\pi}} \sum_{n=1}^{2} \{(-1)^n \alpha \operatorname{Re}[A_n z_n^{\gamma-1}] - \beta \operatorname{Im}[A_n z_n^{\gamma-1}]\}, \\ v_2 &= -\frac{4\gamma\dot{K}}{3\mu\sqrt{\pi}} \sum_{n=1}^{2} \operatorname{Re}[A_n z_n^{\gamma-1}]. \end{aligned} \tag{4.2}$$

A substitution of (4.2) into the first and second terms of expressions (2.2) of the nominal stress rates yields:

$$\begin{aligned} \dot{t}_{11} &= \frac{4\gamma\dot{K}}{3\sqrt{\pi}} (\gamma - 1)(2\xi - k - \eta) \sum_{n=1}^{2} \{(-1)^n \alpha \operatorname{Re}[A_n z_n^{\gamma-2}] - \beta \operatorname{Im}[A_n z_n^{\gamma-2}]\} + \dot{p}, \\ \dot{t}_{22} &= -\frac{4\gamma\dot{K}}{3\sqrt{\pi}} (\gamma - 1)(2\xi + k - \eta) \sum_{n=1}^{2} \{(-1)^n \alpha \operatorname{Re}[A_n z_n^{\gamma-2}] - \beta \operatorname{Im}[A_n z_n^{\gamma-2}]\} + \dot{p}. \end{aligned} \tag{4.3}$$

The hydrostatic stress rate may consequently be determined by the condition of achievement of (2.4) in the form:

$$\dot{p} = \frac{4\gamma\dot{K}}{3\sqrt{\pi}} (\gamma - 1) \sum_{n=1}^{2} \{(-1)^n \alpha [2(1-k)\beta^2 + k] \operatorname{Re}[A_n z_n^{\gamma-2}] + \beta [2(1-k)\alpha^2 - k] \operatorname{Im}[A_n z_n^{\gamma-2}]\}, \tag{4.4}$$

where the relations (2.13) have been used. The complete expressions for the nominal stress rates follow from (4.3) and (4.4) and the third and fourth terms of (2.2)

$$\begin{aligned} \dot{t}_{11} &= \frac{4\gamma\dot{K}}{3\sqrt{\pi}} (\gamma - 1) \sum_{n=1}^{2} \{(-1)^n (\beta\delta + \chi\alpha) \operatorname{Re}[A_n z_n^{\gamma-2}] + (\alpha\delta - \chi\beta) \operatorname{Im}[A_n z_n^{\gamma-2}]\}, \\ \dot{t}_{22} &= \frac{4\gamma\dot{K}}{3\sqrt{\pi}} (\gamma - 1) \sum_{n=1}^{2} \{(-1)^n (\beta\delta - \chi\alpha) \operatorname{Re}[A_n z_n^{\gamma-2}] + (\alpha\delta + \chi\beta) \operatorname{Im}[A_n z_n^{\gamma-2}]\}, \\ \dot{t}_{12} &= -\frac{4\gamma\dot{K}}{3\sqrt{\pi}} (\gamma - 1) \sum_{n=1}^{2} \{(\chi\beta^2 - \chi\alpha^2 + 2\alpha\beta\delta) \operatorname{Re}[A_n z_n^{\gamma-2}] + (-1)^n (\delta\alpha^2 - \delta\beta^2 + 2\chi\alpha\beta) \operatorname{Im}[A_n z_n^{\gamma-2}]\}, \\ \dot{t}_{21} &= -\frac{4\gamma\dot{K}}{3\sqrt{\pi}} (\gamma - 1) \sum_{n=1}^{2} \{\chi \operatorname{Re}[A_n z_n^{\gamma-2}] + (-1)^n \delta \operatorname{Im}[A_n z_n^{\gamma-2}]\}, \end{aligned} \tag{4.5}$$

where

$$\chi = 2\xi - \eta, \quad \delta = 2(1-k)\alpha\beta = \sqrt{4\xi - 4\xi^2 - k^2}. \tag{4.6}$$

4.1. Mode I symmetry conditions

Under Mode I loading conditions, in view of (2.27) and (4.1), the velocity fields (4.3) must be endowed with corresponding symmetry properties, namely:

$$v_1(z_1, z_2) = v_1(\bar{z}_2, \bar{z}_1), \quad v_2(z_1, z_2) = -v_2(\bar{z}_2, \bar{z}_1), \tag{4.7}$$

which imply $A_2 = -\overline{A_1}$, or equivalently

$$A_n = (-1)^n a + \mathrm{i}b \quad (n = 1, 2), \tag{4.8}$$

being a and b real constants.

When the second and fourth terms of expressions (4.5) and the velocity gradient calculated from (4.2) are introduced into the boundary conditions (2.26) on the crack faces (at $\vartheta = \pi$ or, equivalently, $\vartheta_n = \pi$), the following homogeneous system for the real constants a and b may be obtained, using relations (2.19) and (4.8):

$$\begin{aligned} &[(\beta\delta - \alpha\tilde{\chi})a + (\beta\tilde{\chi} + \alpha\delta)b]\cos(\gamma\pi) = 0, \\ &(\delta a - \tilde{\chi} b)\sin(\gamma\pi) = 0, \end{aligned} \tag{4.9}$$

where $\tilde{\chi} = \chi + \sigma_{22}/\mu$ for pressure loading (2.21) or $\tilde{\chi} = \chi$ for dead loading (2.22). If the surface instability condition

$$\alpha\tilde{\chi}^2 - 2\beta\tilde{\chi}\delta - \alpha\delta^2 = 0, \tag{4.10}$$

is excluded, the system (4.9) admits a nontrivial solution for the constants a and b if and only if condition (3.14) is verified. It must be noted that the condition (4.10) occurs for the same critical value k defined by (3.15). Moreover, in the particular case of pressure loading boundary conditions, condition (3.15) results in the relation (3.16) between ξ and k, represented as the dashed curve in Fig. 2.

If the condition (4.10) is excluded, the lowest admissible value of γ given by (3.14) is 3/2 and thus the local crack-tip fields for the nominal and hydrostatic stress rates display the square root singularity, as for the cases considered in Section 3. Moreover, for $\gamma = 3/2$ the second term of condition (4.9) on the crack faces, at $\vartheta = \pi$, yields the following relation between the constants a and b:

$$b = a\delta/\tilde{\chi}. \tag{4.11}$$

Therefore, the leading-order contributions of the various fields can be expressed in terms of a single constant a. The introduction of the angular functions $\boldsymbol{\omega}(\vartheta)$, $\boldsymbol{\tau}(\vartheta)$ and $\rho(\vartheta)$ allows for the representation of the stress and velocity asymptotic fields in the form (3.18). The angular functions can be obtained from (4.2), (4.4) and (4.5) by using (4.8) and (4.11) in the form:

$$
\begin{aligned}
\omega_1(\vartheta) &= 2a\sum_{n=1}^{2}\{(\alpha\tilde{\chi}-\delta\beta)c_n(\vartheta)-(-1)^n(\delta\alpha+\tilde{\chi}\beta)s_n(\vartheta)\},\\
\omega_2(\vartheta) &= -2a\sum_{n=1}^{2}\{(-1)^n\tilde{\chi}c_n(\vartheta)-\delta s_n(\vartheta)\},\\
\tau_{11}(\vartheta) &= a\sum_{n=1}^{2}\{[\beta\delta(\tilde{\chi}-\chi)+\alpha(\chi\tilde{\chi}+\delta^2)]\hat{c}_n(\vartheta)-(-1)^n[\alpha\delta(\tilde{\chi}-\chi)-\beta(\chi\tilde{\chi}+\delta^2)]\hat{s}_n(\vartheta)\},\\
\tau_{22}(\vartheta) &= a\sum_{n=1}^{2}\{[\beta\delta(\tilde{\chi}+\chi)-\alpha(\chi\tilde{\chi}-\delta^2)]\hat{c}_n(\vartheta)-(-1)^n[\alpha\delta(\tilde{\chi}+\chi)+\beta(\chi\tilde{\chi}-\delta^2)]\hat{s}_n(\vartheta)\},\\
\tau_{12}(\vartheta) &= -a\sum_{n=1}^{2}\{(-1)^n[(\chi\tilde{\chi}-\delta^2)(\beta^2-\alpha^2)+2\alpha\beta\delta(\tilde{\chi}+\chi)]\hat{c}_n(\vartheta)\\
&\qquad +[\delta(\tilde{\chi}+\chi)(\beta^2-\alpha^2)-2\alpha\beta(\chi\tilde{\chi}-\delta^2)]\hat{s}_n(\vartheta)\},\\
\tau_{21}(\vartheta) &= -a\sum_{n=1}^{2}(-1)^n(\chi\tilde{\chi}+\delta^2)\hat{c}_n(\vartheta)+\delta(\tilde{\chi}-\chi)\hat{s}_n(\vartheta),\\
\rho(\vartheta) &= a\sum_{n=1}^{2}\{[(\beta\tilde{\chi}+\alpha\delta)\delta+(\alpha\tilde{\chi}-\beta\delta)k]\hat{c}_n(\vartheta)+[(\beta\tilde{\chi}+\alpha\delta)k-(\alpha\tilde{\chi}-\beta\delta)\delta](-1)^n\hat{s}_n(\vartheta)]\},
\end{aligned}
\tag{4.12}
$$

being

$$
\begin{aligned}
g_n(\vartheta) &= \sqrt{[\cos\vartheta+(-1)^n\alpha\sin\vartheta]^2+\beta^2\sin^2\vartheta},\\
c_n(\vartheta) &= \sqrt{g_n(\vartheta)+\cos\vartheta+(-1)^n\alpha\sin\vartheta},\quad \hat{c}_n(\vartheta)=\frac{c_n(\vartheta)}{g_n(\vartheta)},\\
s_n(\vartheta) &= \sqrt{g_n(\vartheta)-\cos\vartheta-(-1)^n\alpha\sin\vartheta},\quad \hat{s}_n(\vartheta)=\frac{s_n(\vartheta)}{g_n(\vartheta)}.
\end{aligned}
\tag{4.13}
$$

Finally, employing the fourth term of (4.12) and using

$$
v_{2,2}(\vartheta) = -\frac{\dot{K}_{\mathrm{I}}}{\mu\sqrt{2\pi r}}a\sum_{n=1}^{2}\{(\alpha\tilde{\chi}-\beta\delta)\hat{c}_n(\vartheta)+(-1)^n(\beta\tilde{\chi}+\alpha\delta)\hat{s}_n(\vartheta)\},
$$

for pressure loading on the crack faces, the normalization condition $\tilde{\tau}_{22}(0)=1$ yields the following expression for the constant a:

$$
a = [2\sqrt{2}(-\alpha\tilde{\chi}^2+2\beta\tilde{\chi}\delta+\alpha\delta^2)]^{-1},
\tag{4.14}
$$

which diverges as the condition (4.10) is verified.

4.2. Mode II symmetry conditions

Under Mode II loading conditions, in view of (2.28) and (4.1), the velocity fields (4.3) must be endowed with corresponding symmetry properties, namely:

$$
v_1(z_1,z_2) = -v_1(\bar{z}_2,\bar{z}_1),\quad v_2(z_1,z_2)=v_2(\bar{z}_2,\bar{z}_1),
\tag{4.15}
$$

which imply $A_2 = \overline{A_1}$, or equivalently

$$A_n = -a - (-1)^n \mathrm{i} b \quad (n = 1, 2), \tag{4.16}$$

being a and b real constants.

When the second and fourth terms of expressions (4.5) are introduced into the boundary conditions (2.26) on the crack faces (at $\vartheta = \pi$ or, equivalently, $\vartheta_n = \pi$), the following homogeneous system for the real constants a and b may be obtained, by using relations (2.19) and (4.16):

$$\begin{aligned} &[(\alpha\delta + \beta\tilde{\chi})a + (\alpha\tilde{\chi} - \beta\delta)b]\sin(\gamma\pi) = 0, \\ &(\tilde{\chi}a + \delta b)\cos(\gamma\pi) = 0. \end{aligned} \tag{4.17}$$

If the condition (4.10) is excluded, system (4.17) admits a nontrivial solution for the constants a and b if and only if condition (3.14) occurs, corresponding to $\gamma = 3/2$. Moreover, the first term of condition (4.17) yields the following relation between the constants a and b:

$$b = \frac{\beta\tilde{\chi} + \alpha\delta}{\beta\delta - \alpha\tilde{\chi}} a. \tag{4.18}$$

Therefore, the leading-order contributions of the various fields can be expressed in terms of a single constant a. The introduction of the angular functions $\boldsymbol{\omega}(\vartheta)$, $\boldsymbol{\tau}(\vartheta)$ and $\rho(\vartheta)$ allows for the representation of the stress and velocity asymptotic fields in the form (3.27). The angular functions can be obtained from (4.2), (4.4) and (4.5) by using (4.16) and (4.18) in the form:

$$\begin{aligned}
\omega_1(\vartheta) &= 2a(\alpha^2 + \beta^2) \sum_{n=1}^{2} \{\delta s_n(\vartheta) + (-1)^n \tilde{\chi} c_n(\vartheta)\}, \\
\omega_2(\vartheta) &= -2a \sum_{n=1}^{2} \{(-1)^n (\beta\tilde{\chi} + \alpha\delta) s_n(\vartheta) + (\alpha\tilde{\chi} - \beta\delta) c_n(\vartheta)\}, \\
\tau_{11}(\vartheta) &= -a(\alpha^2 + \beta^2) \sum_{n=1}^{2} \{\delta(\chi + \tilde{\chi})\hat{s}_n(\vartheta) - (-1)^n (\chi\tilde{\chi} - \delta^2)\hat{c}_n(\vartheta)\}, \\
\tau_{22}(\vartheta) &= -a(\alpha^2 + \beta^2) \sum_{n=1}^{2} \{\delta(\tilde{\chi} - \chi)\hat{s}_n(\vartheta) + (-1)^n (\chi\tilde{\chi} + \delta^2)\hat{c}_n(\vartheta)\}, \\
\tau_{12}(\vartheta) &= a(\alpha^2 + \beta^2) \sum_{n=1}^{2} \{(-1)^n [\alpha\delta(\tilde{\chi} - \chi) + \beta(\chi\tilde{\chi} + \delta^2)]\hat{s}_n(\vartheta) + [\beta\delta(\chi - \tilde{\chi}) + \alpha(\chi\tilde{\chi} + \delta^2)]\hat{c}_n(\vartheta)\}, \\
\tau_{21}(\vartheta) &= a \sum_{n=1}^{2} \{(-1)^n [\alpha\delta(\tilde{\chi} + \chi) + \beta(\chi\tilde{\chi} - \delta^2)]\hat{s}_n(\vartheta) + [\beta\delta(\chi + \tilde{\chi}) - \alpha(\chi\tilde{\chi} - \delta^2)]\hat{c}_n(\vartheta)\}, \\
\rho(\vartheta) &= -a(\alpha^2 + \beta^2) \sum_{n=1}^{2} \{\delta(\tilde{\chi} + k)\hat{s}_n(\vartheta) + (-1)^n (\delta^2 - k\tilde{\chi})\hat{c}_n(\vartheta)\}.
\end{aligned} \tag{4.19}$$

The normalization condition $\tilde{\tau}_{21}(0) = 1$, where

$$v_{2,1}(\vartheta) = a \frac{\dot{K}_{\mathrm{II}}}{\mu\sqrt{2\pi r}} \sum_{n=1}^{2} \{(-1)^n (\beta\tilde{\chi} + \alpha\delta^2)\hat{s}_n(\vartheta) + (\beta\delta - \alpha\tilde{\chi})\hat{c}_n(\vartheta)\},$$

can be used for pressure loading on the crack faces—implies the same expression (4.14) for the constant a, which holds both for Mode I and Mode II loading conditions.

5. Conserved integrals

We begin recalling from Biot (1965) and Hill and Hutchinson (1975) that constitutive Eq. (2.2) admit a velocity gradient potential ϕ, defined in such a way that

$$\dot{t}_{ij} = \frac{\partial \phi}{\partial v_{j,i}} + \dot{p}\delta_{ij}. \tag{5.1}$$

In order to keep into account different boundary conditions on the crack faces, a velocity gradient potential may also be introduced for the fictitious stress rate $\tilde{t}_{ij}$ in the form

$$\tilde{t}_{ij} = \frac{\partial \tilde{\phi}}{\partial v_{j,i}} + \dot{p}\delta_{ij}, \tag{5.2}$$

with

$$\tilde{\phi} = \phi + \tfrac{1}{2}\sigma_2 v_{i,j} v_{j,i}, \tag{5.3}$$

for pressure loading (2.21) and with $\tilde{\phi} = \phi$ for dead loading (2.22).

With the above definition (5.2) of $\tilde{\phi}$, we may introduce the following two integrals, defined on any closed contour Γ of the plane $x_1 - x_2$ (with origin O),

$$\mathscr{J}_\alpha = \int_\Gamma (\tilde{\phi} n_\alpha - n_i \tilde{t}_{ij} v_{j,\alpha})\,\mathrm{d}\Gamma, \quad \mathscr{M}_0 = \int_\Gamma (\tilde{\phi} x_\alpha n_\alpha - n_i \tilde{t}_{ij} v_{j,\alpha} x_\alpha)\,\mathrm{d}\Gamma, \tag{5.4}$$

where $\mathrm{d}\Gamma$ is an arc-length element of Γ.

Eq. (5.4) are the incremental versions of the well-known conserved integrals of the infinitesimal theory (Rice, 1985). Noting that $\tilde{t}_{ij,i} = 0$, the proof of the path independence of (5.4) follows immediately from application of the divergence theorem and from the rate equilibrium together with incompressibility condition.

6. Results

Analytical expressions (3.19), (3.28), (4.12) and (4.19) are employed in this Section to investigate the variation of angular fields, namely, nominal stress rate tensor $\boldsymbol{\tau}$ and velocity $\boldsymbol{\omega}$ as functions of the polar coordinate ϑ. Elliptic complex and elliptic imaginary regimes will be investigated under Mode I and Mode II loading conditions. A uniaxial tensile or compressive pre-stress aligned with the crack is considered, so that $\sigma_2 = 0$ and $\eta = k$.

Note that the fictitious stress fields, which may be written in matrix form as

$$[\tilde{\tau}(\vartheta)] = [\tau(\vartheta)] + \frac{\sigma_2}{\mu}\begin{bmatrix} (\omega_1 \cos\vartheta)/2 - \omega_1' \sin\vartheta & (\omega_1 \sin\vartheta)/2 + \omega_1' \cos\vartheta \\ (\omega_2 \cos\vartheta)/2 - \omega_2' \sin\vartheta & (\omega_2 \sin\vartheta)/2 + \omega_2' \cos\vartheta \end{bmatrix},$$

depend on the current stress only through k. Therefore, results for the stress functions reported below pertain also to pressure loading boundary conditions when components $\tau_{ij}(\vartheta)$ are replaced by $\tilde{\tau}_{ij}(\vartheta)$.

6.1. Elliptic Imaginary regime

The results reported in Figs. 3 and 4 refer, respectively, to Mode I and Mode II loading of a Mooney-Rivlin material, $\xi = 1$. Different values of the pre-stress k have been considered ranging between two ex-

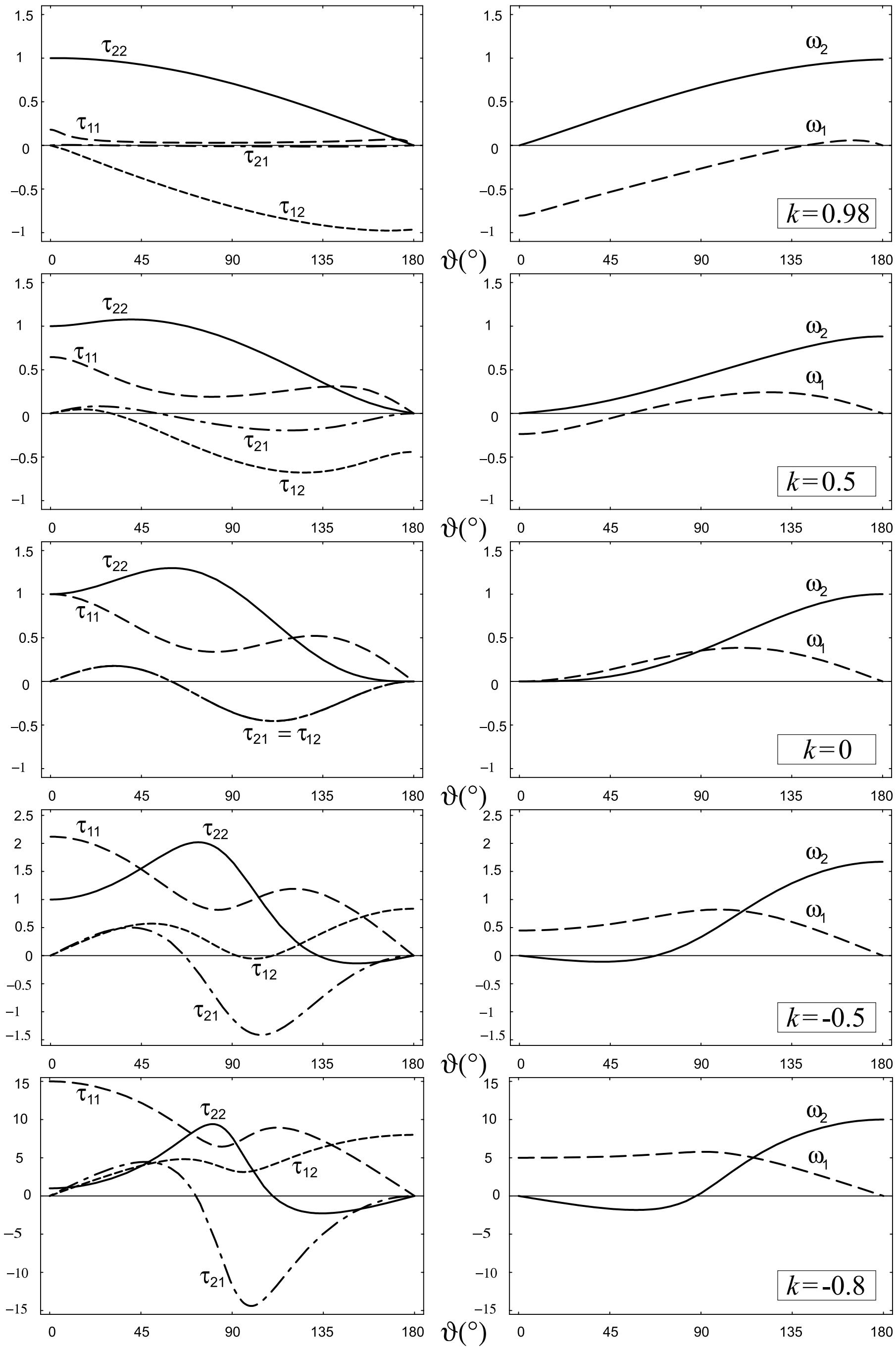

Fig. 3. Angular variation of nominal stress rate and velocity (Cartesian components) for Mode I loading of a Mooney-Rivlin material ($\xi = 1$) at different values of pre-stress k.

treme values; one is close to the (P) boundary in traction ($k = 0.98$) and the other is close to the surface instability in compression ($k = -0.80$). We recall from Biot (1965), Hill and Hutchinson (1975) and Young

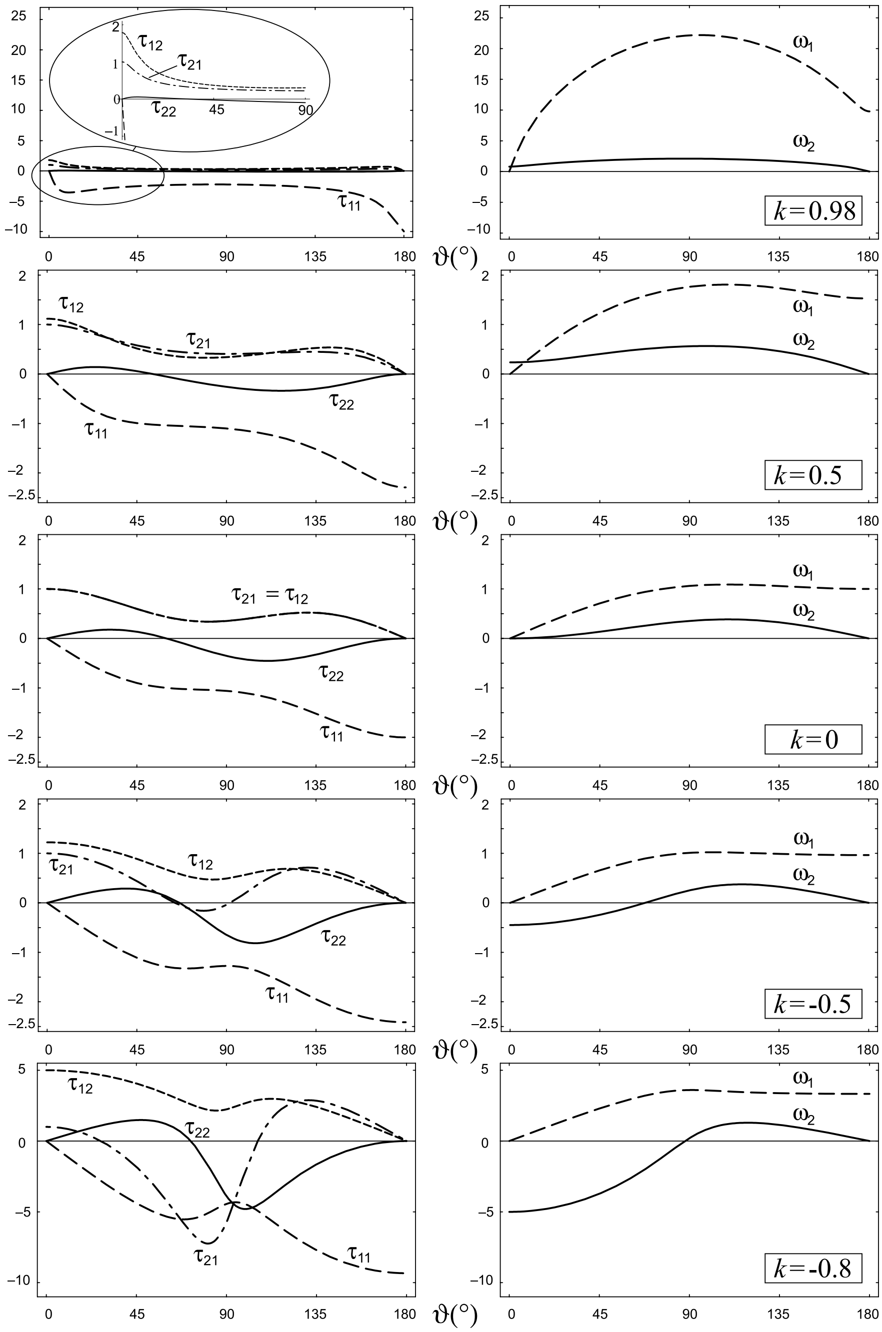

Fig. 4. As for Fig. 3, except that Mode II loading is considered.

(1976) that loss of ellipticity occurs in the limits $k = \pm 1$ and surface instability only occurs in compression, at $k \approx -0.839$. Results relative to values of pre-stress beyond the surface instability threshold are not reported here, but they show that a negative value of $\omega_2(\pi)$ occurs, when the normalization condition

$\tau_{22}(0) = 1$ is considered. This occurrence indicates a physically nonadmissible situation, consequent to the fact that the current configuration is unstable.

The results reported in Figs. 3 and 4 show a strong effect of the pre-stress on all the crack-tip fields. Note that the nominal shear components τ_{12} and τ_{21} are equal only in the absence of pre-stress, $k = 0$. Under Mode I loading conditions, we note from Fig. 3 that a compressive pre-stress increases the crack-tip opening displacement, whereas this tendency is less evident in the component ω_1 under Mode II (Fig. 4).

When k is increased (see the curves relative to $k = 0.98$), the nominal incremental tractions on area elements normal to the reference axes tend to be aligned with the x_2-axis for Mode I, or with the x_1-axis for Mode II. This effect is connected to the appearance of shear bands, formally possible only *at* the elliptic boundary. For an initially isotropic material approaching the (EI)/(P) boundary—as in particular the Mooney-Rivlin material—shear bands are excluded, in the sense that they could only be attained in the limit of infinite stretch, corresponding to $k = \pm 1$. A simple analysis reveals that, when $k = \pm 1$, the shear bands result to be parallel to (or orthogonal to) the pre-stress when this is tensile (or compressive). This means that, in our crack problem, the shear bands are aligned with the crack line, when k approaches 1. As shown by Bigoni and Capuani (2002), even if shear bands are formally excluded within the elliptic domain,

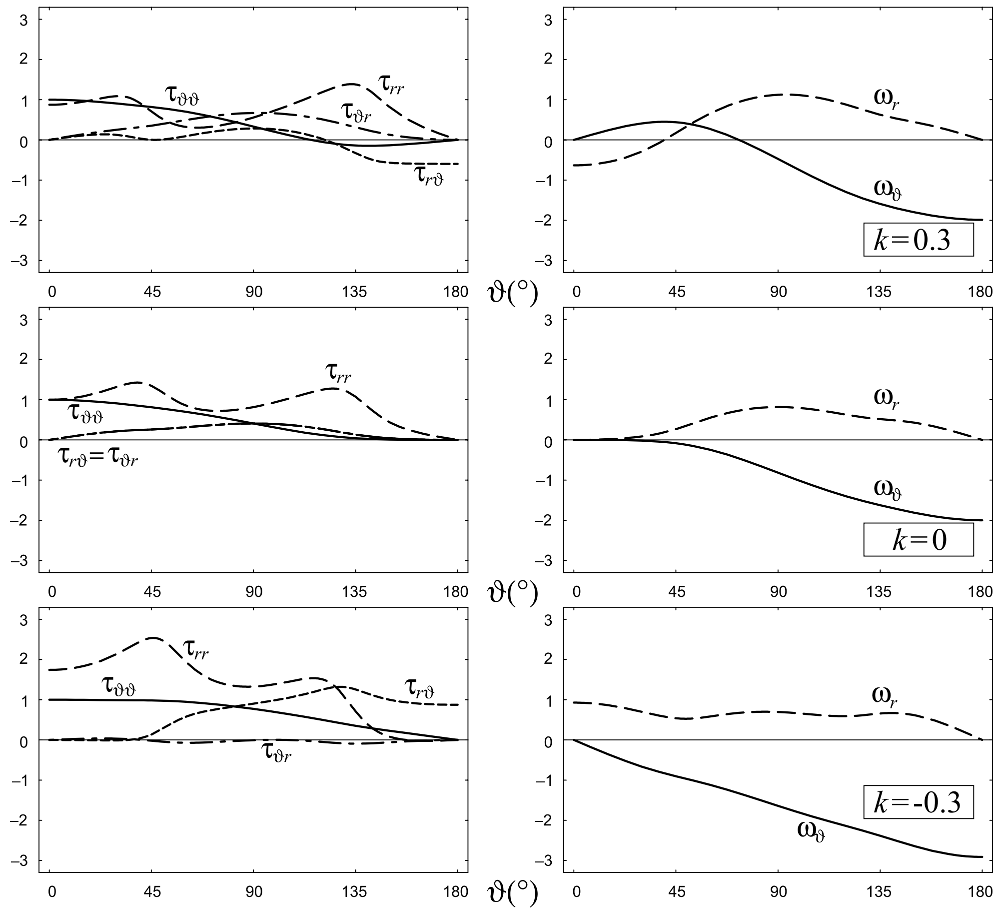

Fig. 5. Angular variation of nominal stress rate and velocity (cylindrical components) for Mode I loading of a material with $\xi = 1/4$ at different values of pre-stress k.

strain localization may occur as induced by a perturbation, applied on a ground state sufficiently close to the elliptic boundary. This conclusion is relevant also here, where incremental strain produced by both Mode I and Mode II loading tends to localize ahead of the crack tip in a band aligned with the crack, a situation resembling crazing in polymers.

6.2. Elliptic complex regime

Stress and velocity fields are reported in Figs. 5 and 6 for Mode I loading conditions in the elliptic complex regime, with $\xi = 1/4$. Mode II loading is considered in Figs. 7 and 8. In these figures, instead of the Cartesian components used in Figs. 3 and 4, the polar components

$$
\begin{aligned}
\omega_r &= \omega_1 \cos\vartheta + \omega_2 \sin\vartheta, \\
\omega_\vartheta &= -\omega_1 \sin\vartheta + \omega_2 \cos\vartheta, \\
\tau_{rr} &= \tau_{11}\cos^2\vartheta + \tau_{22}\sin^2\vartheta + (\tau_{12}+\tau_{21})\cos\vartheta\sin\vartheta, \\
\tau_{\vartheta\vartheta} &= \tau_{11}\sin^2\vartheta + \tau_{22}\cos^2\vartheta - (\tau_{12}+\tau_{21})\cos\vartheta\sin\vartheta, \\
\tau_{r\vartheta} &= -(\tau_{11}-\tau_{22})\cos\vartheta\sin\vartheta + \tau_{12}\cos^2\vartheta - \tau_{21}\sin^2\vartheta, \\
\tau_{\vartheta r} &= -(\tau_{11}-\tau_{22})\cos\vartheta\sin\vartheta + \tau_{21}\cos^2\vartheta - \tau_{12}\sin^2\vartheta,
\end{aligned}
\tag{6.1}
$$

are reported. This facilitates the discussion about strain localization, when approaching the (EC) boundary. Values of pre-stress k have been considered ranging between the two surface instability thresholds, corresponding to $k \approx 0.776$ in tension and $k \approx -0.562$ in compression. These take place well before loss of ellipticity, occurring at $k \approx \pm 0.866$.

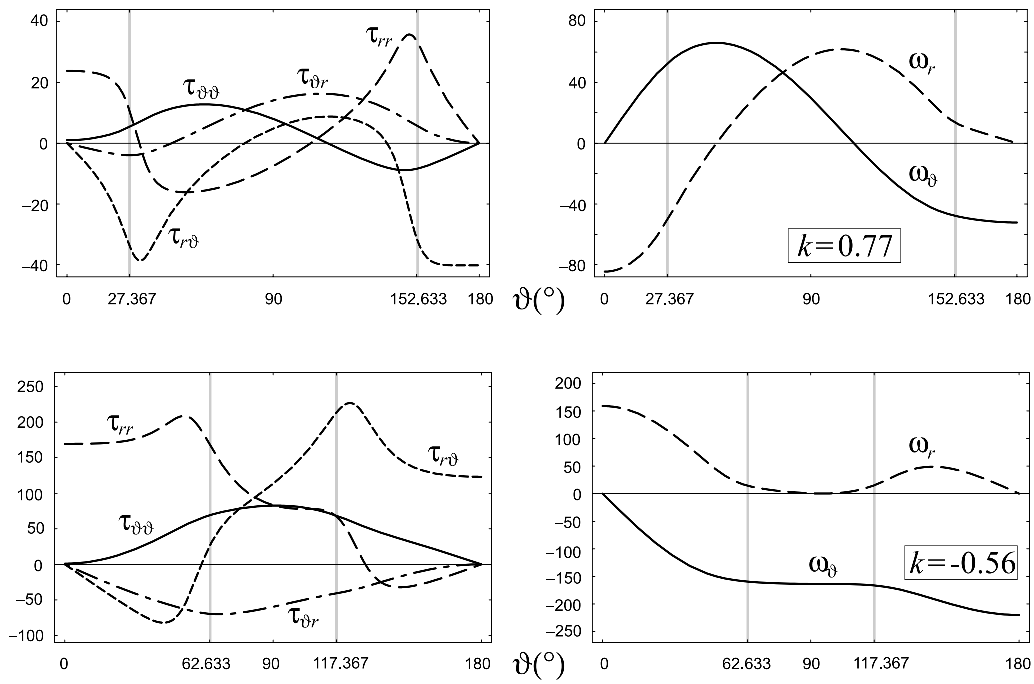

Fig. 6. As for Fig. 5, except that values of pre-stress k close to the instability of crack surface are considered.

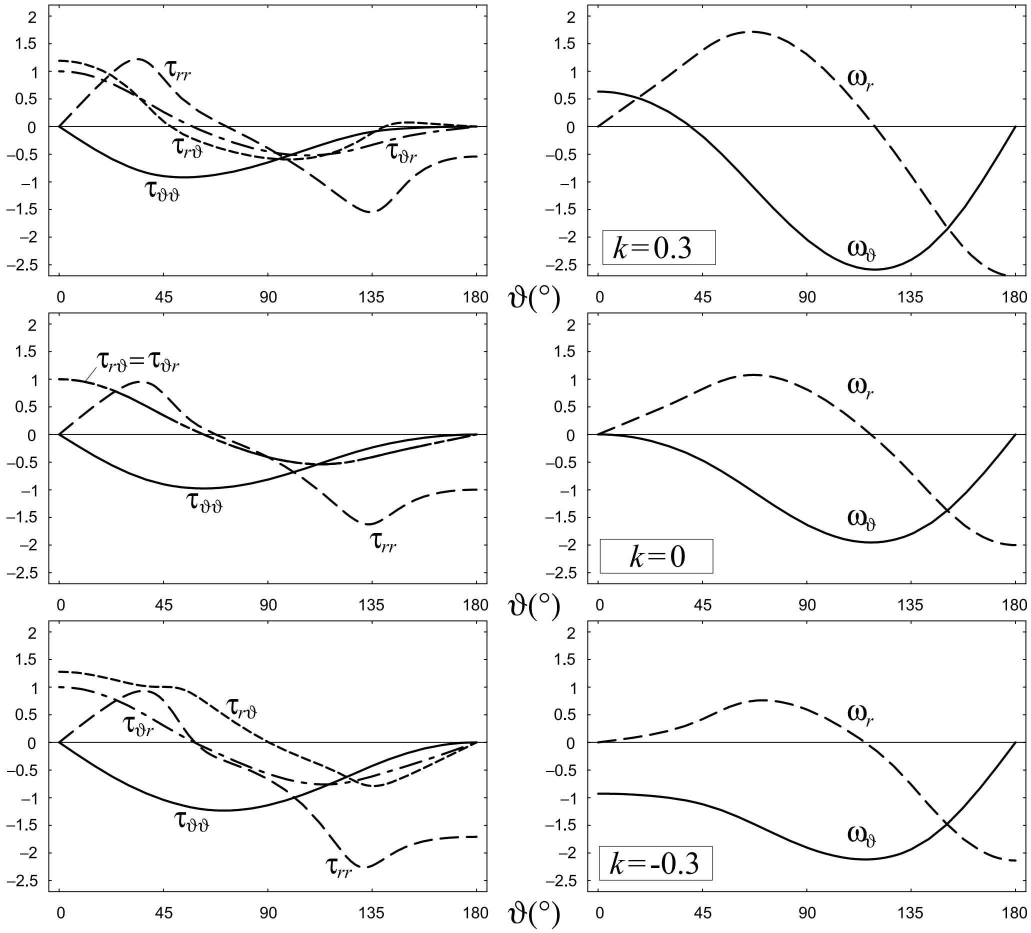

Fig. 7. Angular variation of nominal stress rate and velocity (cylindrical components) for Mode II loading of a material with $\xi = 1/4$ at different values of pre-stress k.

As for the Mooney-Rivlin material, we may note from Figs. 5–8 that the pre-stress has a strong effect on the asymptotic rate fields. The behaviour of these fields in proximity to the surface instability limit is investigated in Figs. 6 and 8, relative to $k = 0.770$ and -0.560.

The different field amplitudes, corresponding to positive and negative values of k should be noted. In the same graphs, the angular coordinates are reported, relative to the shear bands that would form at the (EC)/(H) boundary. In particular (Fig. 9), two shear bands form at the (EC)/(H) boundary, equally inclined with respect to the crack line, at $\vartheta_0 \approx 27.367°$ for tensile pre-stress and at $\vartheta_0 \approx 62.633°$ for compressive pre-stress. As sketched in Fig. 9, equilibrium considerations at discontinuity surfaces reveal that only the two in-plane stress components τ_{rr} and $\tau_{r\vartheta}$ may suffer jumps at (EC)/(H) boundary. The implication in the present asymptotic analysis is that approaching the (EC)/(H) boundary, these stress components tend to increase and undergo sharp variations at ϑ_0 and $\pi - \vartheta_0$. However, loss of ellipticity cannot be achieved without encountering a surface instability. This is closer to the (EC)/(H) boundary in tension than in compression. Therefore, we can appreciate peaks in stress/strain rates along directions corresponding to strain localization in tension, whereas in compression strain localization is still not clearly formed (Figs. 6 and 8).

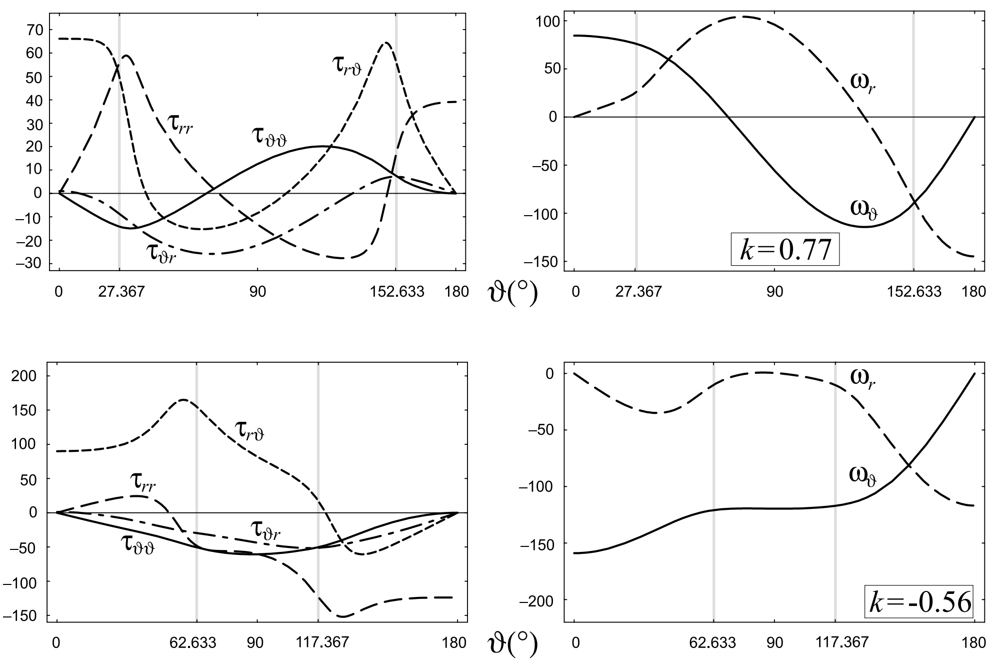

Fig. 8. As for Fig. 7, except that values of pre-stress k close to the instability of crack surface are considered.

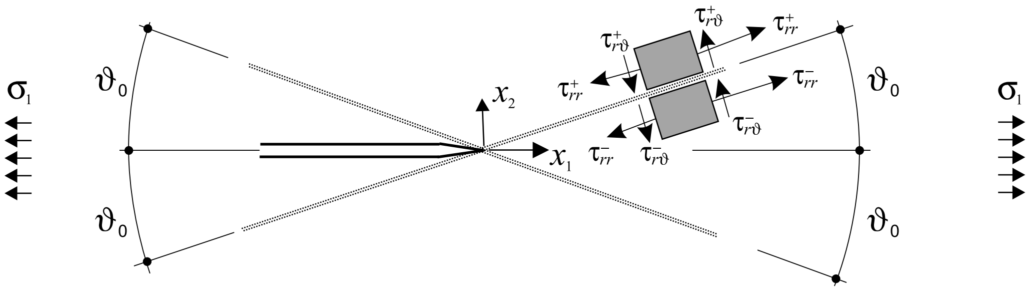

Fig. 9. Shear bands geometry at the crack tip.

6.3. J_2-deformation theory of plasticity

To conclude the investigation, we present results for the J_2-deformation theory of plasticity, which falls within the framework outlined in the previous sections. Briefly, for plane strain deformation, with λ denoting the in-plane stretch parallel to axis x_1 (note that $\lambda > 1$ in tension and $0 < \lambda < 1$ in compression), the J_2-deformation theory corresponds to (Hutchinson and Neale, 1978)

$$\xi = \frac{N}{2\varepsilon\coth(2\varepsilon)}, \quad k = \frac{1}{\coth(2\varepsilon)}, \quad \dot{\sigma}_{33} = \dot{p}, \tag{6.2}$$

where N is a constitutive parameter ranging between 0 and 1 (0 is excluded), $\varepsilon = \ln\lambda$ is the principal logarithmic strain in the direction x_1 and $\dot{\sigma}_{33}$ is the out-of-plane Cauchy stress increment. Moreover, loss of

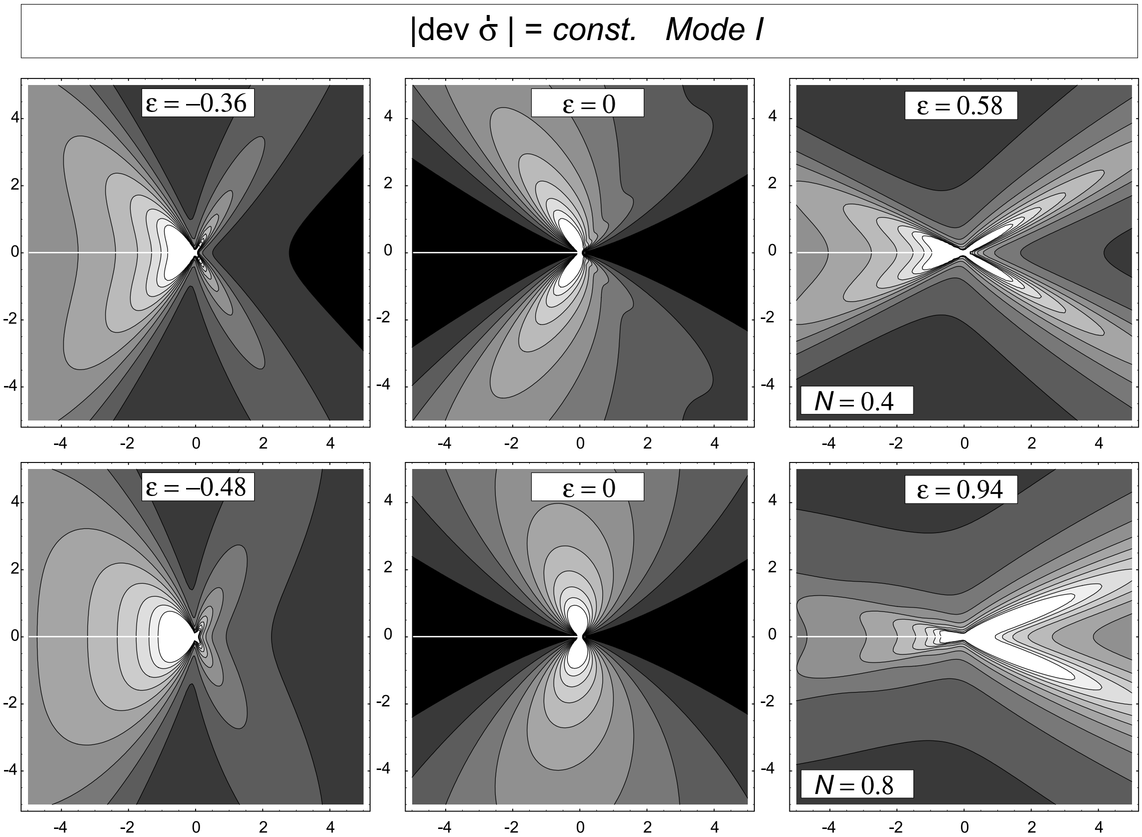

Fig. 10. Level sets of the modulus of deviatoric Cauchy stress rate, for Mode I loading of a J_2-deformation theory material with $N = 0.4$ and 0.8. The crack surface is denoted by a white line.

ellipticity occurs at a critical logarithmic strain ε_c for an inclination ϑ_0 satisfying (Hutchinson and Tvergaard, 1981)

$$\varepsilon_c = [N(2\varepsilon_c \coth(2\varepsilon_c) - N)]^{1/2}, \quad \vartheta_0 = \begin{cases} \pi/2 - \arctan e^{\varepsilon_c} & \text{for } \sigma_1 > 0, \\ \arctan e^{\varepsilon_c} & \text{for } \sigma_1 < 0. \end{cases} \tag{6.3}$$

The critical logarithmic strains ε_s for surface instability may be obtained through substitution of the first and second terms of (6.2) into (3.16), thus obtaining the condition

$$\varepsilon_s(1 - e^{-2\varepsilon_s}) = N, \tag{6.4}$$

a formula derived by Hutchinson and Tvergaard (1980).

Graphs with the variations of angular crack-tip fields are similar to those already shown in Figs. 5–8 and are not reported. Instead, we investigate the increment in the deviatoric component of Cauchy stress rate,

$$\operatorname{dev} \dot{\boldsymbol{\sigma}} = \dot{\boldsymbol{\sigma}} - \tfrac{1}{3}(\operatorname{tr} \dot{\boldsymbol{\sigma}})\mathbf{I}. \tag{6.5}$$

In particular, the level sets of the modulus of deviatoric Cauchy stress increment (6.5) are reported in Figs. 10 and 11 for Mode I and Mode II loading, respectively. The two cases of $N = 0.4$ and 0.8 are investigated. In the former case, loss of ellipticity occurs at $\varepsilon \approx \pm 0.6778$ ($\vartheta_0 = 26.918°$ for $\varepsilon > 0$ and $\vartheta_0 = 63.082°$ for $\varepsilon < 0$) and surface instability corresponds to $\varepsilon \approx 0.5817$ for tension ($\sigma_1 > 0$) and $\varepsilon \approx -0.3679$ for

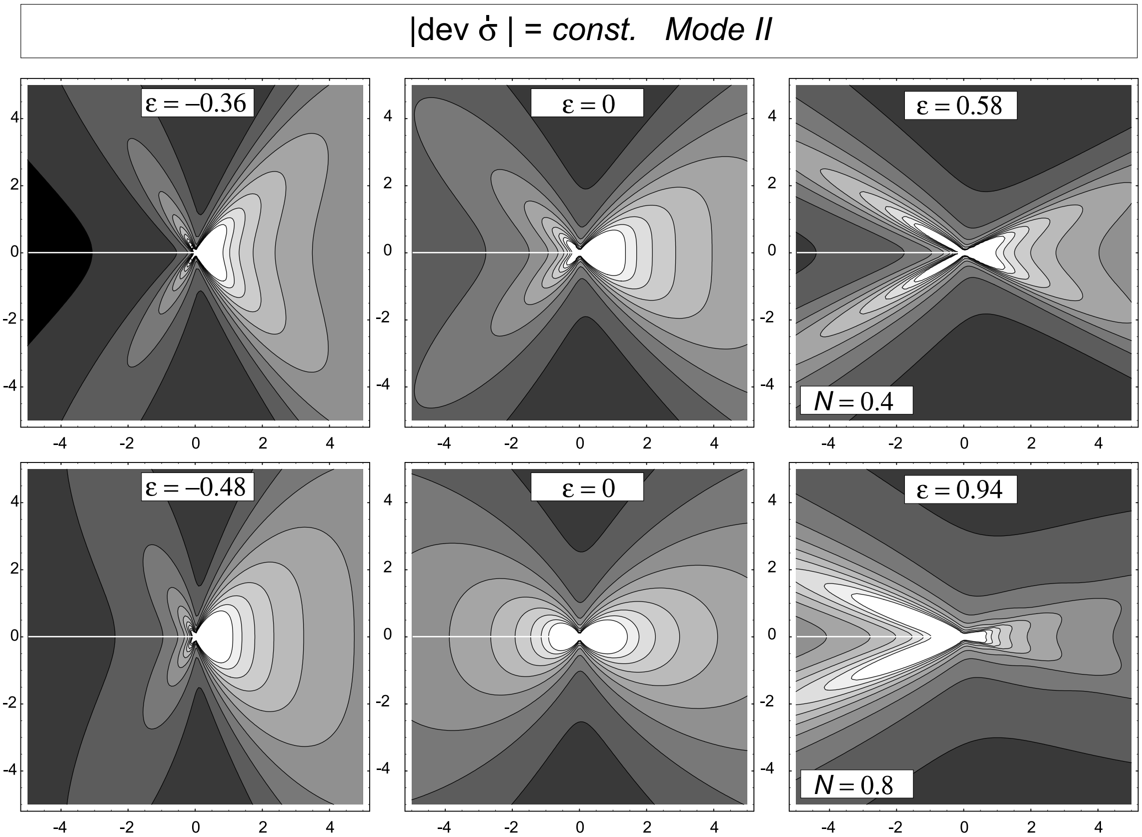

Fig. 11. As for Fig. 10, except that Mode II loading is considered.

compression ($\sigma_1 < 0$). In the latter case, these values become $\varepsilon \approx \pm 1.0324$ ($\vartheta_0 = 19.603°$ for $\varepsilon > 0$ and $\vartheta_0 = 70.397°$ for $\varepsilon < 0$), $\varepsilon \approx 0.9430$ for $\sigma_1 > 0$ and $\varepsilon \approx -0.4863$ for $\sigma_1 < 0$. In addition to the case of null pre-stress, $\varepsilon = 0$, extreme values of ε ($\varepsilon = -0.360, 0.580$, for $N = 0.4$ and $\varepsilon = -0.48, 0.94$, for $N = 0.8$) have been considered, very close to instability of crack surface. For tensile pre-stress, the logarithmic strain ε though close to surface instability, is however not far from loss of ellipticity. Therefore, traces of localization of deformations are clearly visible, ahead of and behind the crack tip for Mode I and Mode II, respectively. Another interesting feature is that for values of ε close to surface instability, the stress-increment maps relative to Mode I and Mode II reveal an unexpected mirror symmetry with respect to axis x_2.

7. Conclusions

The effect of pre-stress on near-tip fields of a stationary crack in a nonlinear, hyperelastic and incompressible material has been investigated. In particular, with reference to a homogeneously and plane strain deformed infinite body containing a crack, a closed-form asymptotic solution has been given for incremental Mode I and Mode II deformations. Two different boundary conditions on the crack faces have been considered, corresponding to a fixed pressure loading or a dead loading. Even if the former condition may be more appropriate, an interesting point has emerged regarding the difference between the two conditions. Particularly, these are shown to lead to two slightly different definitions of stress intensity factor rates and related incremental conserved integrals.

A main finding, also obtained by Soós (1996a) in a somewhat different context, is a square-root singularity for the incremental stress and strain fields, akin to the situation pertaining to the infinitesimal theory. However, differently from the latter, the solution reveals that the pre-stress strongly influences the crack-tip conditions and new features have been given evidence. In particular, the near-tip crack fields undergo significant variations when the limits either of crack faces instability or of shear banding are approached. In the former case, interesting field symmetries emerge whereas, in the latter case, localized deformations become clearly visible.

Acknowledgements

Financial support from M.U.R.S.T. ex60% (2000) and from University of Trento (Trento, Italy) is gratefully acknowledged.

References

Antipov, Y.A., Kolaczkowski, S.T., Movchan, A.B., Spence, A., 2000. Asymptotic analysis for cracks in a catalytic monolith combustor. Int. J. Solids Struct. 37, 1899–1930.

Azhdari, A., Obata, M., Nemat-Nasser, S., 2000. Alternative solution methods for crack problems in plane anisotropic elasticity, with examples. Int. J. Solids Struct. 37, 6433–6478.

Barnett, D.M., Asaro, R.J., 1972. The fracture mechanics of slit-like cracks in anisotropic elastic media. J. Mech. Phys. Solids 20, 353–366.

Bigoni, D., Capuani, D., 2002. Green's function for incremental, nonlinear elasticity: shear bands and boundary integral formulation. J. Mech. Phys. Solids 50, 471–500.

Biot, M.A., 1965. Mechanics of Incremental Deformations. Wiley, New York.

Crăciun, E.M., Soós, E., 1998. Interaction of two unequal cracks in a prestressed fiber reinforced composite. Int. J. Fract. 94, 137–159.

Dowaikh, M.A., Ogden, R.W., 1990. On surface waves and deformations in a pre-stressed incompressible elastic solid. IMA J. Appl. Math. 44, 261–284.

Eshelby, J.D., Read, W.T., Shockley, W., 1953. Anisotropic elasticity with application to dislocation theory. Acta Metallurgica 1, 251–259.

Geubelle, P.H., 1995. Finite deformation effects in homogeneous and interfacial fracture. Int. J. Solids Struct. 32, 1003–1016.

Geubelle, P.H., Knauss, W.G., 1994. Finite strains at the tip of a crack in a sheet of hyperelastic material: I. Homogeneous case. J. Elast. 35, 61–98.

Green, D.J., Maloney, B.R., 1986. Influence of surface stress on indentation cracking. J. Am. Ceram. Soc. 69, 223–225.

Hill, R., Hutchinson, J.W., 1975. Bifurcation phenomena in the plane tension test. J. Mech. Phys. Solids 23, 239–264.

Hutchinson, J.W., Neale, K.W., 1978. Sheet necking. II. Time independent behavior. In: Koistinen, D.P., Wang, N-M. (Eds.), Mechanics of Sheet Metal Forming. Plenum Press, New York, pp. 127–153.

Hutchinson, J.W., Tvergaard, V., 1980. Surface instabilities on statically strained plastic solids. Int. J. Mech. Sci. 22, 339–354.

Hutchinson, J.W., Tvergaard, V., 1981. Shear band formation in plane strain. Int. J. Solids Struct. 17, 451–470.

Knowles, J.K., Sternberg, E., 1973. An asymptotic finite-deformation analysis of the elastostatic field near the tip of a crack. J. Elast. 3, 67–107.

Knowles, J.K., Sternberg, E., 1974. Finite-deformation analysis of the elastostatic field near the tip of a crack: reconsideration and higher order results. J. Elast. 4, 201–233.

Lawn, B.R., Marshall, D.B., 1977. Contact fracture resistance of physically and chemically tempered glass plates. Phys. Chem. Glasses 18, 7–18.

Le, K.Ch., Stumpf, H., 1993. The singular elastostatic field due to a crack in rubberlike materials. J. Elast. 32, 183–222.

Lekhnitskii, S.G., 1981. Theory of Elasticity of an Anisotropic Body. Mir Publisher, Moscow.

Loret, B., Radi, E., 2001. On dynamic crack growth in poroelastic fluid-saturated media. J. Mech. Phys. Solids 49, 995–1020.

Needleman, A., Ortiz, M., 1991. Effect of boundaries and interfaces on shear-band localization. Int. J. Solids Struct. 28, 859–877.

Obata, M., Nemat–Nasser, S., Goto, Y., 1989. Branched cracks in anisotropic elastic solids. J. Appl. Mech. 56, 858–864.
Ogden, R.W., 1984. Non-linear Elastic Deformations. Ellis Horwood, Chichester.
Piva, A., Radi, E., 1991. Elastodynamic local fields for a crack running in an orthotropic medium. J. Appl. Mech. 58, 982–987.
Rice, J.R., 1974. Limitation to the small scale yielding approximation of elastic plastic crack-tip fields. J. Mech. Phys. Solids 22, 17–26.
Rice, J.R., 1985. Conserved integrals and energetic forces. In: Bilby, B.A., Miller, K.J., Willis, J.R. (Eds.), Fundamentals of Deformation and Fracture (Eshelby Memorial Symposium). Cambridge University Press, pp. 33–56.
Sih, G.C., Paris, P.C., Irwin, G.R., 1965. On cracks in rectilinearly anisotropic bodies. Int. J. Frac. Mech. 1, 189–203.
Soós, E., 1996a. Resonance and stress concentration in a prestressed elastic solid containing a crack. An apparent paradox. Int. J. Eng. Sci. 34, 363–374.
Soós, E., 1996b. Stability, resonance and stress concentration in prestressed piezoelectric crystals containing a crack. Int. J. Eng. Sci. 34, 1647–1673.
Stephenson, R.A., 1982. The equilibrium field near the tip of a crack for finite plane strain of incompressible elastic materials. J. Elast. 12, 65–99.
Young, N.J.B., 1976. Bifurcation phenomena in the plane compression test. J. Mech. Phys. Solids 24, 77–91.
Willis, J.R., 1966. Hertzian contact of anisotropic bodies. J. Mech. Phys. Solids 14, 163–176.
Wong, F.S., Shield, R.T., 1969. Large plane deformations of thin elastic sheets of neo-Hookean material. Z. Angew. Math. Phys. 20, 176–199.